




Cite this: *Soft Matter*, 2018, 14, 7483

# Role of fingerprint-inspired relief structures in elastomeric slabs for detecting frictional differences arising from surface monolayers†

Charles Dhong, \* Laure V. Kayser, Ryan Arroyo, Andrew Shin, Mickey Finn III, Andrew T. Kleinschmidt and Darren J. Lipomi \*

The perception of fine texture of an object is influenced by its microscopic topography and surface chemistry—*i.e.*, the topmost layer of atoms and molecules responsible for its surface energy, adhesion, and friction generated when probed by a fingertip. Recently, it has been shown that human subjects can discriminate high-energy (*i.e.*, hydrophilic), oxidized silicon from low-energy (*i.e.*, hydrophobic), fluorinated alkylsilane-coated silicon. The basis of discrimination was consistent with differences between stick-slip friction frequencies generated when sliding the fingertip across the two surfaces. One aspect that was not examined was the presence of surface relief structures on the fingertip. Indeed, papillary ridges—fingerprints—may be involved in enhanced discrimination of fine textures arising from surface roughness, but how (or whether) fingerprints may also be involved in the discrimination of surface chemistry—through its effect on friction—is unknown. Here, using a mock finger made from a slab of silicone rubber shows that relief structures amplify differences in stick-slip friction when slid across either a hydrophilic oxide or a hydrophobic monolayer on silicon. We quantify the similarity between the friction traces of the mock fingers sliding across hydrophilic and hydrophobic surfaces under varying velocities and applied masses using a cross-correlation analysis. We then convert the cross-correlational data into convenient “discriminability matrices.” These matrices identify combinations of downward forces and sliding velocities that enhance differences in friction between hydrophilic and hydrophobic monolayers. In addition, a computational model of macroscopic, “rate-and-state” friction confirms that frictional differences in chemistry are amplified when elastic slabs bear a patterned interface. This biomimetic approach to engineering sliding interfaces may inform the development of improved electronic skin and haptic devices and may contribute to understanding the role of relief structure in tactile perception.

Received 15th June 2018,  
Accepted 17th August 2018

DOI: 10.1039/c8sm01233d

[rsc.li/soft-matter-journal](http://rsc.li/soft-matter-journal)

## Introduction

The animal kingdom is replete with examples of relief structures on the skin that confer adaptive advantages: the structures on the toes of geckos<sup>3</sup> and tree frogs<sup>4,5</sup> enhance grip, while the hairs on the feet of water striders allow the animals to sit atop a pond.<sup>6,7</sup> Koalas and the great apes—including humans—have papillary ridges (fingerprints) on their fingers and toes. Experiments in which rubber “mock fingers” with and without relief structures were slid across rough surfaces produced complex tangential forces. These time-dependent, oscillatory forces were markedly different from those generated in the absence of relief structures (“fingerprints”).<sup>8,9</sup> The implication was that fingerprints may play a role in tactile discrimination of fine texture (whether or not this discrimination was ever the basis for natural selection in

evolution). The “feel” of an object, however, is influenced not only by its surface roughness, but also by its surface chemistry—*i.e.*, differences in atomic and molecular structure that influence surface energy, which in turn influences friction and adhesion. Here, we show that relief structures on a silicone rubber slab amplify the differences in tangential forces when slid across surfaces terminated by different molecular species, specifically, an oxidized silicon wafer and a silane-passivated one. Our findings are supported with a model based on a “rate-and-state”<sup>10,11</sup> description of friction. These results provide clues for understanding the role of surface structure in the tactile sense and may lead to new design principles for prostheses and haptic interfaces.<sup>12</sup>

## Background

Humans have a remarkable ability to discriminate fine texture. Skedung *et al.*<sup>13</sup> showed that human subjects can differentiate flat polymeric surfaces from those bearing periodic wrinkles

Department of NanoEngineering, University of California, San Diego, La Jolla, CA, USA. E-mail: [cbdhong@eng.ucsd.edu](mailto:cbdhong@eng.ucsd.edu), [dlipomi@eng.ucsd.edu](mailto:dlipomi@eng.ucsd.edu)

† Electronic supplementary information (ESI) available. See DOI: 10.1039/c8sm01233d

with amplitudes as small as 10 nm. Human subjects are not thought to be sensitive to the heights of these wrinkles, however, but rather to the vibrational frequencies generated by sliding the finger over the wrinkles.<sup>13</sup> Later, Skedung *et al.* and Gueorguiev *et al.*<sup>14</sup> found that human subjects can discriminate surfaces based on differences in friction arising from roughness,<sup>13</sup> while our laboratory has shown that subjects can also differentiate surfaces by surface chemistry alone.<sup>2</sup> The tactile cue in both cases was believed to be vibrations generated by friction.

The vast majority of studies connecting the chemistry of molecular monolayers to friction have done so with remarkable sensitivity but on the microscopic scale. These studies generally use atomic force microscopy (AFM) or sophisticated surface force apparatuses.<sup>15–19</sup> Microscale friction, however, is only qualitatively related to the friction acting over the cm<sup>2</sup>-areas characteristic of human touch.<sup>20</sup> There are relatively few studies that have isolated the effect of self-assembled monolayers on friction at this larger scale.<sup>15,16</sup> These approaches, moreover, were not focused on the friction generated by deformable, patterned objects reminiscent of fingertips.

The mechanics describing the ways that fingertips slide across surfaces (in which the surface chemistries were unmodified) have been the subject of a large body of work.<sup>9,21–23</sup> During a typical measurement, the friction force exhibits oscillations characteristic of stick-slip behaviour. This complex behaviour cannot be encapsulated by coefficients of static friction found in a table. These values have, however, been used in a two-term model,<sup>9</sup> which can account for some key features of the observed behaviour. (For example, how the contact area between a finger and substrate is modified by friction which varies with time.) Nevertheless, a constant static coefficient of friction still cannot be used to predict the vibrations caused by stick-slip events.<sup>24,25</sup>

One approach that relates surface chemistry to the vibrations generated by friction is a “rate-and-state” model.<sup>11,26,27</sup> This model is applicable to macroscopic systems and recognizes that the friction coefficient is dependent on both velocity (“rate”) and path (history or “state”). This model is not typically used in viscoelastic interfaces such as the motion of an untreated, tacky silicone rubber sliding across a rigid substrate. The skin’s outer layer (stratum corneum), however, is glassy, even when moist (dry, 0.1 GPa and wet, 0.06 GPa<sup>28</sup>) and moderately hydrophobic (~60°, water contact angle).<sup>29</sup> As the finger is not tacky, rate-and-state models can be used to describe stick-slip friction. In the “stick” portion, the tangential force between two surfaces builds up until motion begins. One surface then undergoes a rapid motion (“slip”) until the surface “sticks” again, and the cycle repeats. Repeating cycles of stick-slip produce vibrations. The frequency and amplitude of these vibrations depend on the roughness and surface chemistry of the two sliding surfaces; they also depend on the sliding velocity and the normal force. Critically, if one surface, such as a finger, is deformable (~100 kPa), stick-slip can occur simultaneously at different locations on the finger.<sup>21</sup> These “slip” events can occur in unison (“global slip”<sup>30</sup>) or discordantly (“partial” or “local” slip).

Stick-slip vibrations are transduced into neuronal events by tactile corpuscles. In glabrous skin, there are four types of these

corpuscles which differ in structure, by the frequencies that they detect, and by their depth in the dermis.<sup>31</sup> They are the slow-adapting Merkel and Ruffini corpuscles, found at the surface and the deep dermis, respectively, along with the fast-adapting Meissner and Pacinian corpuscles, also found at the surface and the deep dermis, respectively. Scheibert *et al.* has investigated how fingerprint-like ridges can alter the friction generated on rough surfaces; these ridges modify the vibrational signals believed to be detected by the Meissner and Pacinian corpuscles.<sup>32</sup> Specifically, the authors performed experiments in which a hemispherical surface bearing fingerprint-like ridges enhanced vibrations arising from rough surfaces more so than did hemispheres without “fingerprints”. A curious finding of this work was that the largest enhancements in vibrations in smooth vs. ridged fingers occurred in the range of frequencies detected by the Pacinian corpuscles. At the same time, vibrational frequencies detected by the Meissner corpuscles were damped by the finger bearing ridges. This result suggested that the Pacinian corpuscles were most responsible for discriminating rough surfaces. The Pacinian corpuscles, however, are found in the deep dermis, whereas the Meissner corpuscles are found near the surface of the skin.<sup>31,33,34</sup> One of the goals of this project was thus to connect the fingerprint-induced modification to the changes to the frequencies of stick-slip friction detected by the different tactile corpuscles, or at least to suggest a framework with which these connections may be investigated by others.

## Experimental design and methods

### Testing apparatus and force sensors

A schematic diagram of the experimental setup is shown in Fig. 1a. We sought to simulate the differences in friction that a human subject would experience by engaging with surfaces with contact areas on the order of ~1 cm<sup>2</sup>. Measurements obtained on this macroscopic scale are less sensitive to contamination from dust and variations in device alignment than are obtained by measurements using microscopic techniques, *e.g.*, AFM. We modeled the finger as a rectangular prism (1 cm × 1 cm × 5 cm) with an area of contact with the substrate of 1 cm<sup>2</sup>. We chose a rectangular geometry because the contact area between a rectangular slab and a surface is independent of load.<sup>35,36</sup> This level of control is not possible for hemispherical or cylindrical geometries.<sup>36</sup> We brought the poly(dimethylsiloxane) (PDMS) slab, loaded with the desired additional mass (*M*), into contact until 1 cm of the finger was touching the wafer from the side view. The finger was then slid a distance of 4 mm using a motorized linear actuator (Newmark Systems) at a constant velocity (*v*) four times across a stationary substrate. We chose the length of the sliding distance based on the fact that human subjects are unlikely to explore at a constant velocity during a longer slide. In addition, studies by Carpenter *et al.*<sup>2</sup> observed that some human subjects rapidly slid their finger in short distances across silicon wafers during free exploration.

The force trace from the first of four sliding events was discarded because it may have been subjected to extraneous

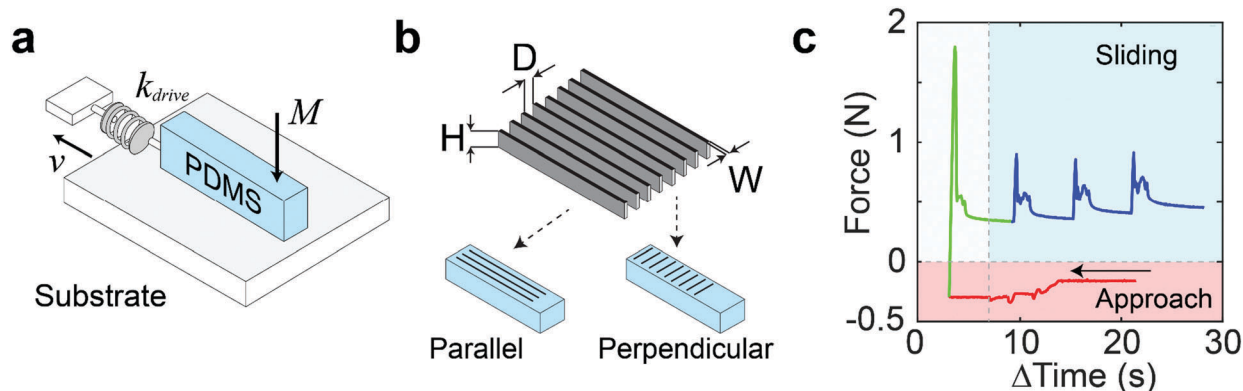


**Fig. 1** Schematic diagram of the apparatus. (a) Force sensor (spring constant,  $k$ ) of velocity,  $v$ , measures tangential forces on PDMS "mock finger" with applied mass  $M$ . (b) PDMS finger has ridges of width ( $W = 150 \mu\text{m}$ ), pitch ( $D = 350 \mu\text{m}$ ), and height ( $H = 20 \mu\text{m}$ ). Ridges oriented parallel or perpendicular, relative to sliding direction. (c) Typical testing cycle, approach phase (right-to-left) in red, and four discrete pulling events (left-to-right).

adhesive pressure or aging while bringing the mock finger into contact with the substrate (see Fig. 1c). Thus, the finger was slid a total distance of 16 mm, but the friction traces were acquired from the last 12 mm. Residue consisting of silicone was deposited after each sliding event (Fig. S1, ESI†) and thus we repeated the procedure on three fresh spots for every type of mock finger, silicon wafer, sliding velocity, and loading force. A new mock finger was slid several times prior to collection of data to reduce the amount of residue generated during tests and each mock finger was used within 72 h of fabrication. In addition, testing conditions, including the type of mock finger, were varied randomly to ensure repeatability between different masses and velocities.

Tangential forces were measured using a Futek 250 g LSB, connected to a Keithley 2611b sampling at  $55 \text{ s}^{-1}$  with a peak-to-peak noise of 0.1 mN. The spring constant of the sensor was  $13.9 \text{ kN m}^{-1}$  and the finger was approximated with a spring constant of  $0.3 \text{ kN m}^{-1}$ , based on the force–displacement relationship of a rectangular slab in simple shear.

#### Fabrication of PDMS slabs and fingerprint-inspired relief structures

There are several approaches in the literature to model the fingertip as it engages with a surface.<sup>37</sup> The most appropriate of these models depends on the mode of engagement (*e.g.* tapping<sup>38</sup> *vs.* sliding). A complicating factor is that the mechanical properties of skin are nonuniform as a function of depth. The effective modulus of a fingertip ( $E = 70\text{--}200 \text{ kPa}$ <sup>39</sup>) is similar to that of a very soft elastomer, but, because of the keratinous surface layer, it is not adhesive (as is the native surface of silicone rubber). The interface between the finger and a surface is thus characterized by contact points that are rigid and glassy. These can be modelled as a network of microscopic contacts that form and break at multiple locations<sup>11</sup> (rate-and-state models).

We followed standard procedures of soft lithography to produce relief structures in PDMS. To fabricate the slabs, we poured PDMS into 3D-printed molds. The rectangular molds also contained a 3D-printed cylindrical "bone" (diameter = 2.5 mm) suspended midway with a screw to provide structural support to the PDMS slab. We mixed the PDMS (Sylgard 184, Dow Corning)

at a ratio of 30:1 (base to crosslinker by mass) to mimic the effective Young's modulus of real fingers (including layering effects of underlying bone, different skin layers, *etc.*) of  $\sim 100 \text{ kPa}$ .<sup>39</sup> The acrylic mold, with an acrylic "bone" inside, was placed on top of a wafer coated with poly(methylmethacrylate) (PMMA) (5% w/w PMMA/anisole) and then PDMS was poured into the mold. The PMMA/anisole facilitated release of the PDMS finger by rinsing with acetone. Depending on the type of PDMS slab, these wafers were either planar or patterned with ridges photolithographically (SU-8 2050, Microchem) oriented to be parallel or perpendicular to the sliding direction. PDMS was cured in an oven at  $60^\circ\text{C}$  for 2 h. The PDMS slabs had ridges that had a width,  $W$ , of  $150 \mu\text{m}$ , with a pitch,  $D$ , of  $350 \mu\text{m}$ , and a height,  $H$ , of  $20 \mu\text{m}$  (see Fig. 1b). We elected not to replicate a real fingerprint because of the high variability between individuals, and limited our experiments to one width, pitch and height of fingerprints.<sup>40</sup> The previous literature has addressed the effect of spacing and aspect ratios on friction.<sup>41,42</sup> Our experiments, in contrast, focused on the effects of velocity, mass, orientation of the ridges, and—critically—surface chemistry (surface energy) of the surface being probed. By using relief structures that were both parallel and perpendicular to the direction of travel, it was possible to understand the behavior of more complex shapes (such as spirals or whorls) present in actual fingerprints.

#### Surface treatment of PDMS slabs

We approximated the stiff, partially hydrophobic,<sup>43</sup> stratum corneum of the skin by oxidizing the surface of the PDMS slabs. We minimized the viscoelastic tack of the native surface of PDMS<sup>44</sup> with UV/ozone (Novascan) for 4 h to crosslink the surface. We then waited at least 1 d before testing. We delayed testing because the UV/ozone initially renders the PDMS hydrophilic. Hydrophobic recovery eventually reverts the PDMS<sup>45</sup> to a similar water contact angle of measurements on human skin (very roughly  $50^\circ$ ), which corresponds to a range of surface energies from  $12 \text{ mJ m}^{-2}$  to  $40 \text{ mJ m}^{-2}$ .<sup>29</sup>

#### Treatment of the wafer surfaces

The SiOH layer was created by exposing bare silicon to an air plasma in a plasma chamber (PDC-001-HP, Harrick) for 5 min

at 300 mTorr. Plasma-treated wafers (referred to as “SiOH”) were prepared freshly before testing and used within 2 h. Passivation using (1H,1H,2H,2H-tridecafluorotetrahydrooctyl) trichlorosilane (FOTS) was achieved by taking the plasma-treated wafer and placing it into a vacuum desiccator with  $\sim 20 \mu\text{L}$  of FOTS. The wafers were exposed to FOTS under static vacuum for 2 h. Plasma-treating wafers before FOTS deposition produced substrates with roughness similar to the oxidized wafers.<sup>2</sup>

## Results and discussion

### Friction measurements of mock fingers on hydrophilic and hydrophobic wafers

An example of force trace we obtained is shown in Fig. 2a. The parameters were  $M = 75 \text{ g}$  and a drive velocity of the finger,  $v = 7.5 \text{ mm s}^{-1}$ . We show the traces for PDMS slabs without ridges (top panel), with slabs bearing ridges perpendicular to the sliding motion (middle panel) and with ridges parallel to sliding motion (bottom panel) on both FOTS (red) and SiOH (blue). In all traces, we observed oscillations, which are evidence of stick-slip friction. Without stick-slip friction, each trace would reach a plateau and then remain flat. The force traces obtained using slabs without ridges (top panel) are similar between SiOH and FOTS. The perpendicular ridges on the SiOH surface (middle panel, Fig. 2a, blue line) show a small peak, after which the force drops to a steady value. This peak signifies a barrier to the initiation of sliding. Interestingly, it is absent in the force traces obtained on FOTS. In contrast, the parallel ridges show a larger peak for both the FOTS and SiOH (bottom panel). For these parallel ridges, the FOTS peak is even

larger than SiOH. This is surprising because FOTS has a lower surface energy than SiOH, so a view that a lower surface energy should lead to lower friction appears to be overly simplistic. Under these conditions, the SiOH surface (higher friction) might actually be perceived by human subjects as “smoother” than fingers slid on FOTS because the FOTS has a larger peak than SiOH, and that peak disrupts a periodic, even vibration. Of all the experimental results shown in Fig. 2a, we see the greatest variation in amplitude for the PDMS slab with parallel ridges. We note that these observations pertain only to a single set of conditions of loading force and velocity (1 of 16 conditions tested).

We used cross-correlation analysis to quantify the similarity (or difference) between force traces obtained on SiOH *versus* those obtained on FOTS. There are competing views of whether the entire force trace is involved in the tactile discrimination of fine texture, or whether only a segment of the force trace is sufficient. For example, Gueorguiev *et al.*<sup>14</sup> have segmented the force traces into separate regimes of partial slip and full slip, (steady sliding). The authors correlated the friction traces during steady sliding to the ability of human subjects to discriminate surfaces apart based on frictional cues. On experiments with mice, however, Jadhav *et al.*<sup>46</sup> found that incipient motion at a whisker formed some of the basis for neuronal stimulation. This observation suggests that incipient motion, or partial slip, may be a relevant tactile cue. The analysis here uses the entire friction trace, but we have also analysed our results using only the steady sliding regime in the ESI† (see Fig. S3).

The cross-correlational analysis (see Fig. S6–S21 in the ESI† for results obtained for all 16 conditions) is shown to the right

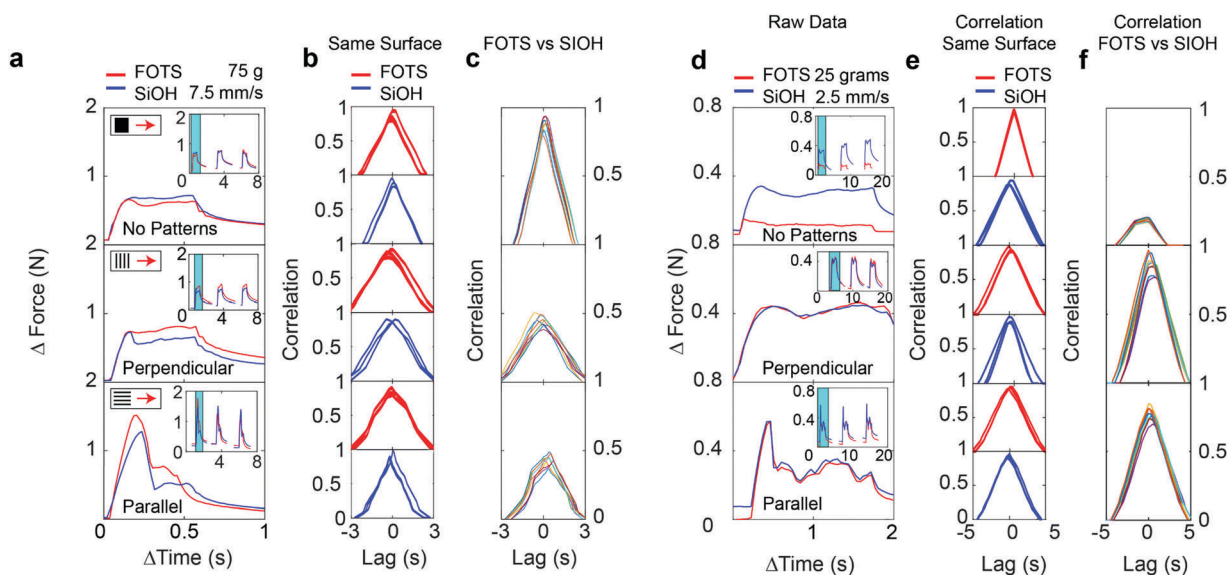


**Fig. 2** Friction forces generated by PDMS slabs on silicon and quantification of their similarities. (a) Force traces generated by PDMS slabs with no ridges (top), and slabs with ridges either perpendicular (middle) or parallel (bottom) to direction of motion. (For this set of data, the conditions were as follows: applied mass,  $M = 75 \text{ g}$ , drive velocity,  $v = 7.5 \text{ mm s}^{-1}$ .) Slabs were tested on silanized (FOTS, red) or oxidized (SiOH, blue) silicon wafers. Insets show additional trials. (b) Cross-correlation of friction traces between trials on the same substrate, as a measure of consistency. (c) Cross-correlation between friction traces on SiOH and FOTS. (d) Force traces of a PDMS slab with applied mass  $M = 25 \text{ g}$ , drive velocity,  $v = 2.5 \text{ mm s}^{-1}$ , (e) the cross-correlation on the same substrate (f) and cross-correlation between SiOH and FOTS.



(Fig. 2b) of the corresponding force traces. The cross-correlation is calculated by:

$$\text{Cross-correlation} = \sum_t [(a(t) - \bar{a}) \times (b(t - \text{lag}) - \bar{b})] \quad (1)$$

where  $a$  and  $b$  are two force traces as a function of time,  $t$ , that were being compared and were calculated about their average values. We normalized the cross-correlation of friction traces by the larger auto-correlation (thus the correlation values plotted in Fig. 2b, c, e and f do not necessarily normalize to 1). When  $a$  and  $b$  were from the different trials under the same conditions, we calculated a reference point for the cross-correlation on the same substrate, seen in Fig. 2b. We also compared the cross-correlation from traces on different substrates (Fig. 2c) to quantify the effect of changing the surface chemistry. A high and symmetric plot of the cross-correlation indicates that the two force traces are similar, while a low and asymmetric plot indicates that the force traces are different. (Our central hypothesis was that the greater the difference between force traces, the greater the probability that the surfaces could be discriminated by touch.)

We observed a high cross-correlation on the same substrate for all mock fingers, which indicates consistency between trials (Fig. 2b).

When considering the cross-correlation between FOTS and SiOH obtained using PDMS slabs with different structures, as in Fig. 2c, the cross-correlation obtained using the slabs with ridges is lower than when using slabs with no ridges. This indicates a higher degree of difference in frictional vibrations for mock fingers with ridges. These results support the hypothesis that relief structures enhance discrimination of FOTS and SiOH by increasing differences in friction forces.

Relief structures do not, however, increase differences under every combination of mass and velocity. In Fig. 2d ( $M = 25$  g,  $v = 2.5$  mm s<sup>-1</sup>), ridges oriented parallel or perpendicular no longer increased differences between SiOH and FOTS, as seen by the overlapping force traces and the large, symmetric cross-correlation. Interestingly, the force traces of the PDMS slabs with parallel ridges (Fig. 2d, bottom), fluctuate with a medium frequency oscillation unseen in the other traces. The force trace has become apparently more complex, with several new peaks. This complexity, however, cannot be regarded as the basis for increased discriminability, because the same features are seen in traces obtained on both FOTS and SiOH (red and blue traces). Therefore, while the PDMS slabs with parallel ridges have generated a more complex force trace, the cross-correlation in Fig. 2f (bottom panel) shows that the traces have become less distinct between FOTS and SiOH, as compared to the conditions in Fig. 2c (bottom panel). The two testing conditions (Fig. 2a–c vs. Fig. 2d–f) gave contrary conclusions about whether ridges enhance differences in friction. Due to the complex dependence of friction on testing conditions, it was necessary to examine a range of conditions ( $M = 0$  to 100 g,  $v = 1$  to 10 mm s<sup>-1</sup>, 16 combinations of conditions, total).<sup>41,47</sup>

## Visualizing the discriminability in friction traces due to topographic ridges

We sought to visualize the cross correlation between all friction traces generated between FOTS and SiOH. Under a given condition, the mock finger generates nine friction traces on each surface. By comparing every friction trace, we generated 81 cross-correlations for each type of PDMS slab (perpendicular ridge, parallel ridges, or no ridges), applied mass and velocity. The average cross-correlation of these 81 comparisons can be quantified using two parameters: “correlation” and “skew”, shown in Fig. 3a–c. Correlation is the total area under the curve, and skew is a measure of the symmetry. In the extremes, the maximum value for the area under the curve is 0.5, given by a perfectly triangular correlation curve, and the minimum value for a perfectly symmetric correlation curve has a skew of zero. We combined these two parameters to construct a “discriminability matrix”, which can be used to visualize the conditions under which the friction traces between FOTS and SiOH are more or less similar.<sup>2</sup> These matrices are shown for PDMS slabs with ridges of all types in Fig. 3d. For mock fingers with “no ridges,” (Fig. 3d, left) the relatively high correlation and low skew means that the force traces obtained on FOTS and SiOH surfaces are similar. This similarity suggests that two surfaces are not discriminable on the basis of friction for that particular set of conditions. For example, for the PDMS slab with ridges perpendicular (Fig. 3d, middle) or parallel (Fig. 3d, right), many regions have turned from red to yellow, or from red to green (compared to Fig. 3d, left, in which the interface had no ridges). This result indicates that the force traces on FOTS and SiOH are more distinct when ridges are present in the PDMS slabs. We thus refine our conclusions to say that for most conditions tested, the ridges on the PDMS slabs lead to an increase in the differences in friction traces between FOTS and SiOH surfaces. In fact, if we superimpose the discriminability of parallel and perpendicular ridges, all conditions show improved discriminability vs. the data obtained with planar slabs. Although superimposing parallel and perpendicular ridges is a simplification for the whorls and spirals in a real fingerprint, this experiment suggests how engaging with a surface along multiple axes can combine to improve discriminability under a wide range of loading forces and velocities. The general conclusion that relief structures in these PDMS “mock fingers” increase differences in friction is true even if we divide the force traces into segments and examine only the middle portion consisting of steady sliding (see ESI,† Fig. S3).

## Origins of increased frictional differences arising from surface relief structures

It is notoriously difficult to replicate the stick-slip friction traces in mock finger experiments using a model<sup>35</sup> without resorting to fitting parameters. The real value of modelling in our case is, instead, to show how the presence of a patterned moving slab might accentuate differences in friction between surfaces. We modeled the sliding of PDMS slabs on the FOTS and SiOH-treated wafers using an elastic (Burridge–Knopoff),<sup>48,49</sup> “rate-and-state” friction model.<sup>1,50</sup> We used the most basic description of a patterned interface by designating every third

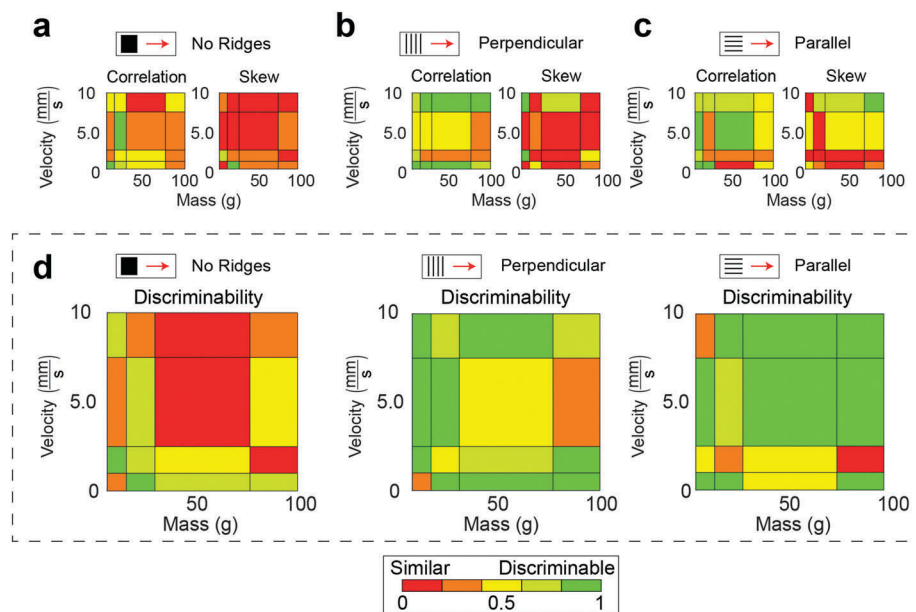


**Fig. 3** Visualizing differences in friction traces with discriminability matrices. Discriminability matrices quantify the similarity between friction traces on SiOH and FOTS. (a) Quantifying the cross-correlations between FOTS and SiOH friction traces. Two metrics used are the normalized area under the curve ('correlation') and the normalized symmetry ('skew') "No Ridges" taken from ref. 2. Matrices (b) for perpendicular ridges and (c) parallel ridges. (d) Discriminability matrix, which combines parametric values of 'correlation' and 'skew' into one matrix. In matrices, red indicates high similarity between force traces on FOTS and SiOH while green indicates low similarity (*i.e.*, high discriminability).

block as a frictionless interconnect to represent the space between ridges in the experimental system, schematically shown in Fig. 4a–c. (When describing the model, we call the blocks which remain in contact with the surfaces "ridges"—in quotation marks—as there is not actually any topography in the model.) The model parameters can be found in Table S2 (ESI†). The "stick-slip" friction is given on each block as:

$$\frac{F_{\parallel}}{F_N} = \mu = \left( \mu_0 + \theta + A \ln \left( \frac{v}{v_c} \right) \right) \quad (2)$$

$$\frac{d\theta}{dt} = \left( -\frac{v}{d_c} \right) \left( \theta + B \ln \left( \frac{v}{v_c} \right) \right) \quad (3)$$

$$\frac{dx}{dt} = v \quad (4)$$

where  $x$  is the position of each block,  $t$  is time,  $\mu$  is the time-varying friction coefficient,  $v_c$  is the drive velocity,  $\theta$  is a component of the time-varying friction that accounts for "state".<sup>1,11</sup> "State" approximates whether the system is in a "stick" phase (with high friction) or a "slip phase" (with low friction).  $A$ ,  $B$  and  $d_c$  are friction parameters, which are not fitting parameters:  $A$  and  $B$  are tabulated from the literature<sup>16,51</sup> and are related to surface chemistry. Higher-energy surfaces, like SiOH, will yield higher values of  $A$  and  $B$ , whereas lower-energy surfaces, like FOTS, have lower values. The parameter  $d_c$

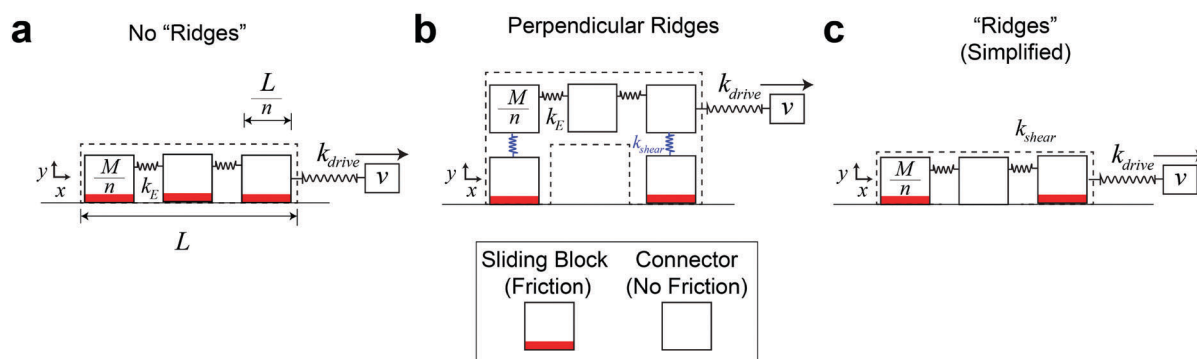


**Fig. 4** "Rate-and-State" friction model of the finger. A finger, which experiences sliding friction, is pulled to positive  $x$  direction at velocity  $v$  attached to a force sensor  $k_{\text{drive}}$ . (a) The finger is broken into discrete elements, or blocks, connected by a spring,  $k_E$ , to approximate an elastic body. Every block (red) experiences "rate-and-state" friction.<sup>1</sup> (b) A finger with "ridges" contains segments do not experience friction (without the red bar) and serve only to connect other blocks. (c) A simplified, equivalent version of the finger with "ridges" for 2D sliding. The applied mass is divided into each block equally.

represents a characteristic slip length, which qualitatively depends on the roughness of the sample and substrate; as we only change surface chemistry, we did not vary  $d_c$  within these calculations.<sup>2</sup> Although  $A$  and  $B$  were measured for a silicon MEMS device in contact with substrates that were nearly identical to those used here, this is, in fact, similar to our mock finger and a real finger. The local glassy exterior of the finger approaches hardness on the order of GPa<sup>28</sup> and the UV/ozone-treated mock finger,<sup>45</sup> a real finger<sup>29</sup> and the MEMS device (SiO<sub>2</sub>)<sup>52</sup> all had approximately similar values of the water contact angle ( $\sim 50^\circ$ ).

These blocks are connected to each other by a spring with spring constant  $k_{\text{shear}}$  to account for elasticity of the finger. Stick-slip events appear as changes in position that deviate from bulk motion ( $v_c \times t$ ). This model can be used to predict the spatiotemporally varying vibrations (*i.e.* tactile stimuli) that a surface generates in a sliding finger.<sup>24</sup> Fig. 5a shows the finger subdivided into blocks and color scheme representing the position on the finger sliding on SiOH (blue) or FOTS (red). The relative position—motion of the block at a velocity other than the imposed drive velocity ( $v$ )—is shown schematically in Fig. 5b. Outputs of the model under one condition,  $v = 10$  mm

$\text{s}^{-1}$  and  $M = 25$  g, are shown in Fig. 5c for a PDMS slab with no “ridges” on SiOH (blue, top panel) and FOTS (red, bottom panel). The relative position show periodic (Schallamach)<sup>53,54</sup> waves that move through the finger. These stick-slip oscillations develop sooner for the SiOH than the FOTS and vary more in amplitude and frequency than does the trace obtained on FOTS. The fact that oscillations are most different at the beginning of the test suggests that the easiest discrimination between FOTS and SiOH surfaces occurs within a short sliding distances of 0.7 mm ( $0.07 \text{ s} \times 10 \text{ mm s}^{-1}$ ). In the case of the blocks with “ridges” in Fig. 5d, we see that oscillations on SiOH and FOTS are delayed, compared to the case where the PDMS slab is modeled without “ridges.” Notably, the plots obtained for FOTS take considerably longer times to develop, reaching the steady-state amplitude at nearly 0.14 s, as compared to 0.08 s for SiOH. This creates a longer time in which FOTS and SiOH have a large difference in friction, which improves the likelihood of discrimination.

### Relevance of friction model to mechanoreceptors

We converted the friction predicted by the model to strain by numerically differentiating the relative position of the blocks. We then applied filters<sup>31</sup> to these strains to determine the strength and frequency of vibrations generated at four different ranges of frequencies on FOTS or SiOH (Fig. 6). As mentioned above, there are four types of tactile corpuscles in the fingertip which each have receptivity centered within a specific range of vibrational frequencies. The Merkel and Ruffini corpuscles respond to static deformations and coarse details of surfaces ( $\sim 1$  mm), with frequencies of  $< 3$  Hz and  $< 5$  Hz, respectively. The Meissner and Pacinian corpuscles, however, can respond to vibrations (fine details and differences), with frequency ranges of 5–50 Hz and 40–400 Hz, respectively. It is possible to quantify the similarity of these filtered, oscillatory signals generated between FOTS and SiOH in each range of frequencies by calculating their cross-correlation. For fingers with no “ridges” (Fig. 6a), the vibrations generated on SiOH and FOTS had a net correlation of  $8.29 \times 10^{-11}$  in the range of 5–50 Hz (Meissner corpuscle). In contrast, the frequencies in the range of 40–400 Hz (Pacinian corpuscle) were much more strongly correlated,  $8.00 \times 10^{-8}$ . The autocorrelation, or a measure of what constitutes a “similar” signal, of the unfiltered strain traces is  $\sim 1 \times 10^{-4}$  (Table S4 and Fig. S5, S6, ESI†). Recalling that larger correlation means greater similarity in the frictional forces when sliding a PDMS slab (or finger) across of a surface, our result suggests that discriminability is greatest in the range of 5–50 Hz. While this analysis is speculative, it is at least consistent with the physiology of the fingertip, in which the Meissner corpuscles are near the surface of the skin and localized around the papillary ridges. The model further shows that the PDMS slab bearing ridges generated larger differences between SiOH and FOTS as compared to the case of no “ridges” ( $1.24 \times 10^{-11}$  versus  $8.29 \times 10^{-11}$ ). These computational results are thus consistent with our experimental finding that soft structures bearing topographic structures increases differences in friction arising from surface energy of a substrate.

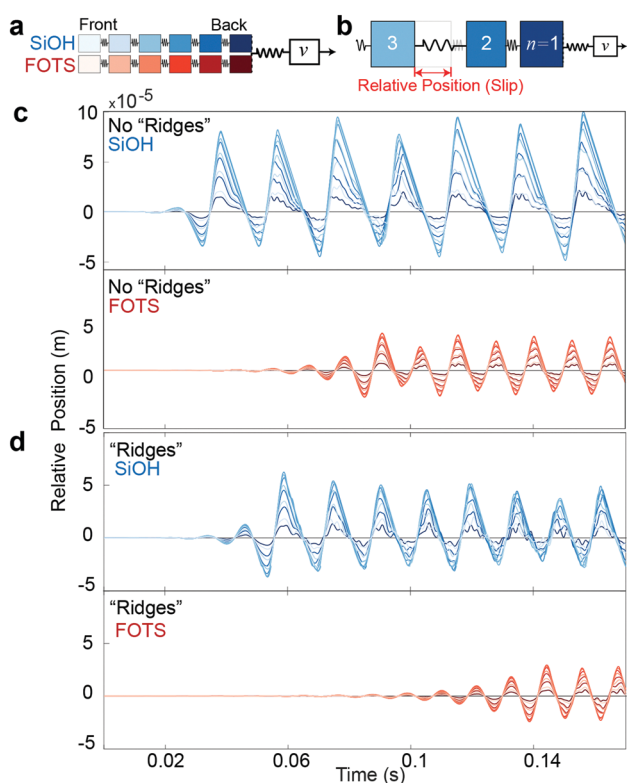


**Fig. 5** Stick-slip friction generated by “rate-and-state” friction model. (a) A finger discretized into blocks and the relative spatial location on the finger indicated by the shade of the color. The color represents the substrate the finger is sliding against (red for FOTS, blue for SiOH). (b) Friction causes blocks to move at different velocities than the motor. At a given time, this discrepancy is known as the relative position or slip. (c) Relative position of a sliding PDMS slab, with no “ridges,” on SiOH (blue) and FOTS (red) and (d) relative position of a PDMS slab bearing “ridges” for  $v = 10 \text{ mm s}^{-1}$  and  $M = 25$  g. Zero represents finger traveling at the drive velocity,  $v$ .

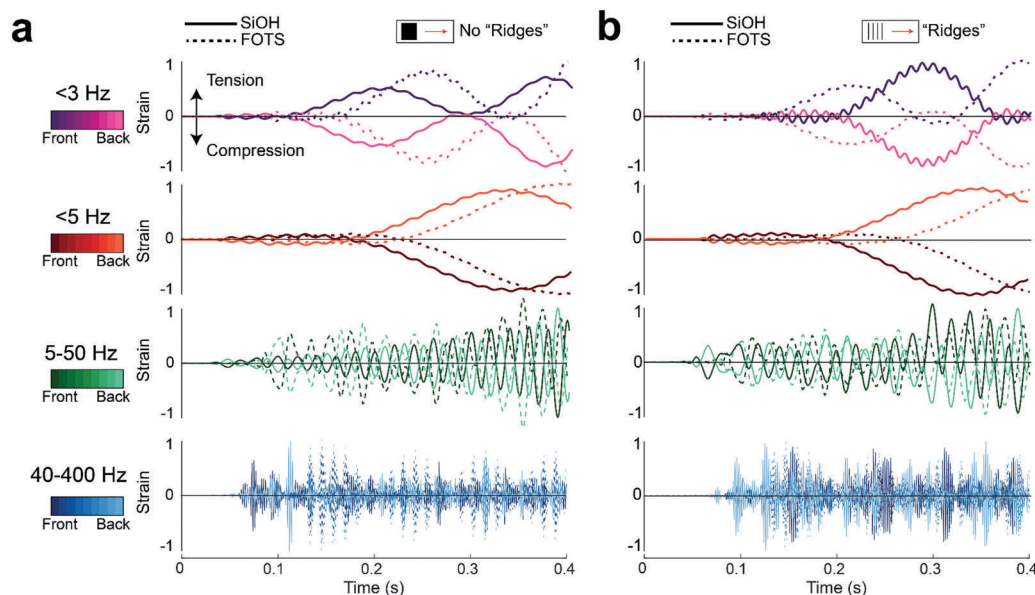


**Fig. 6** Stick-slip friction filtered into different frequency ranges. Strain predicted by “rate-and-state” model was filtered into frequency ranges. These ranges were selected because of their relevance to the four tactile corpuscles found in the fingertip. (a) Differences in strain between SiOH (solid lines) and FOTS (dashed lines) for a finger with no “ridges”. (b) Differences in strain between SiOH (solid lines) and FOTS (dashed lines) for a finger with “ridges.”  $v = 10 \text{ mm s}^{-1}$  and  $M = 25 \text{ g}$ .

## Conclusions

This study investigated how the presence of fingerprint-inspired relief structures may improve tactile discrimination of objects differing only by the chemistry of the surfaces. We demonstrated that PDMS slabs bearing such ridges enhanced differences in the friction generated between hydrophilic (SiOH) and hydrophobic (FOTS) surfaces. We found that ridges oriented parallel and perpendicular each enhanced friction under different conditions of loading force and velocity, and that by combining cues from both orientations increased frictional differences in all conditions tested. It is logical that enhanced differences between frictional forces would be tantamount to increased tactile discrimination in mammals.

We supported these findings with a rate-and-state model, which also showed that an interface between two materials in which the soft material bears periodic surface relief structures amplified differences in friction between hydrophobic and hydrophilic surfaces. Further, we suggested a way in which the friction forces could be filtered into ranges of frequencies. This approach may enable—with the appropriate model—researchers to attribute discrimination carried out with specified loading forces and velocities to specific tactile corpuscles. This methodology could help improve designs for prostheses, electronic skin, haptic devices, soft robots, and other human-machine interfaces by specifying the relevant forces and surface energies needed to elicit a desired mechanical response in a complex, patterned, soft structure—*i.e.*, the skin.

## Conflicts of interest

There are no conflicts to declare.

## Acknowledgements

This work was supported by the NIH Director's New Innovator Award, Grant 1DP2EB022358-03. We acknowledge Dr Vlado Lubarda and Dr Franke Talke for discussions on sliding friction, and Sam Edmunds and Dr Kara Marshall for discussions on filtering and mechanoreceptors, respectively. We also acknowledge Dr Samuel Root for editing the manuscript.

## Notes and references

- 1 A. Ruina, *J. Geophys. Res.: Solid Earth*, 1983, **88**, 10359–10370.
- 2 C. W. Carpenter, C. Dhong, N. B. Root, D. Rodriguez, E. E. Abdo, K. Skelil, M. A. Alkhadra, J. Ramirez, V. S. Ramachandran and D. J. Lipomi, *Mater. Horiz.*, 2017, 70–77.
- 3 K. Autumn, M. Sitti, Y. A. Liang, A. M. Peattie, W. R. Hansen, S. Sponberg, T. W. Kenny, R. Fearing, J. N. Israelachvili and R. J. Full, *Proc. Natl. Acad. Sci. U. S. A.*, 2002, **99**, 12252–12256.
- 4 G. Hanna, W. Jon and W. J. Barnes, *J. Exp. Biol.*, 1991, **155**, 103–125.
- 5 C. Dhong and J. Fréchet, *Soft Matter*, 2015, **11**, 1901–1910.
- 6 X. Gao and L. Jiang, *Nature*, 2004, **432**, 36.
- 7 Y. Zheng, H. Lu, W. Yin, D. Tao, L. Shi and Y. Tian, *Langmuir*, 2016, **32**, 10522–10528.
- 8 P. H. Warman and A. R. Ennos, *J. Exp. Biol.*, 2009, **212**, 2016–2022.
- 9 M. J. Adams, S. A. Johnson, P. Lefèvre, V. Lévesque, V. Hayward, T. André and J.-L. Thonnard, *J. R. Soc., Interface*, 2013, **10**, 20120467.
- 10 A. Ruina and J. Rice, *J. Appl. Mech.*, 1983, **50**, 343–349.
- 11 T. Baumberger and C. Caroli, *Adv. Phys.*, 2006, **55**, 279–348.
- 12 F. L. Hammond, R. K. Kramer, Q. Wan, R. D. Howe and R. J. Wood, *Soft tactile sensor arrays for micromanipulation*,



- IEEE/RSJ International Conference on Intelligent Robots and Systems (IROS), IEEE, 2012, pp. 25–32.
- 13 L. Skedung, M. Arvidsson, J. Y. Chung, C. M. Stafford, B. Berglund and M. W. Rutland, *Sci. Rep.*, 2013, **3**, 2617.
  - 14 D. Gueorguiev, S. Bochereau, A. Mouraux, V. Hayward and J.-L. Thonnard, *Sci. Rep.*, 2016, **6**, 25553.
  - 15 O. Khatri, D. Devaprakasam and S. Biswas, *Tribol. Lett.*, 2005, **20**, 235–246.
  - 16 A. D. Corwin, M. D. Street, R. W. Carpick, W. R. Ashurst, M. J. Starr and M. P. De Boer, Sandia report SAND2005-7954, Sandia National Laboratories, Albuquerque, CA, USA, 2006.
  - 17 T. Ederth, P. Claesson and B. Liedberg, *Langmuir*, 1998, **14**, 4782–4789.
  - 18 V. V. Tsukruk and V. N. Bliznyuk, *Langmuir*, 1998, **14**, 446–455.
  - 19 H. I. Kim, T. Koini, T. R. Lee and S. S. Perry, *Langmuir*, 1997, **13**, 7192–7196.
  - 20 A. Vanossi, N. Manini, M. Urbakh, S. Zapperi and E. Tosatti, *Rev. Mod. Phys.*, 2013, **85**, 529.
  - 21 S. Tomlinson, R. Lewis and M. Carré, *Wear*, 2009, **267**, 1311–1318.
  - 22 D. J. Meyer, M. A. Peshkin and J. E. Colgate, *Fingertip friction modulation due to electrostatic attraction*, World Haptics Conference (WHC), IEEE, 2013, pp. 43–48.
  - 23 S. S. Robinson, K. W. O'Brien, H. Zhao, B. N. Peele, C. M. Larson, B. C. Mac Murray, I. M. Van Meerbeek, S. N. Dunham and R. F. Shepherd, *Extreme Mech. Lett.*, 2015, **5**, 47–53.
  - 24 O. Ben-David and J. Fineberg, *Phys. Rev. Lett.*, 2011, **106**, 254301.
  - 25 L. Skedung, K. Danerlöv, U. Olofsson, M. Aikala, K. Niemi, J. Kettle and M. W. Rutland, *Tribol. Lett.*, 2010, **37**, 389–399.
  - 26 A. D. Berman, W. A. Ducker and J. N. Israelachvili, *Langmuir*, 1996, **12**, 4559–4563.
  - 27 S. S. Shroff and M. P. de Boer, *Tribol. Lett.*, 2016, **63**, 1–15.
  - 28 Y. Yuan and R. Verma, *Colloids Surf., B*, 2006, **48**, 6–12.
  - 29 A. Mavon, H. Zahouani, D. Redoules, P. Agache, Y. Gall and P. Humbert, *Colloids Surf., B*, 1997, **8**, 147–155.
  - 30 C. Schwarz, *Trends Neurosci.*, 2016, **39**, 449–462.
  - 31 R. S. Johansson and J. R. Flanagan, *Nat. Rev. Neurosci.*, 2009, **10**, 345–359.
  - 32 J. Scheibert, S. Leurent, A. Prevost and G. Debrégeas, *Science*, 2009, **323**, 1503–1506.
  - 33 J. A. Pruszynski and R. S. Johansson, *Nat. Neurosci.*, 2014, **17**, 1404–1409.
  - 34 M. Paré, A. M. Smith and F. L. Rice, *J. Comp. Neurol.*, 2002, **445**, 347–359.
  - 35 J. Gao, W. D. Luedtke, D. Gourdon, M. Ruths, J. N. Israelachvili and U. Landman, *J. Phys. Chem. B*, 2004, **108**, 3410–3425.
  - 36 J. N. Israelachvili, *Intermolecular and surface forces*, Academic Press, 2011.
  - 37 B. Bhushan and W. Tang, *J. Appl. Polym. Sci.*, 2011, **120**, 2881–2890.
  - 38 J. Van Kuilenburg, M. Masen, M. Groenendijk, V. v. Bana and E. Van Der Heide, *Tribol. Int.*, 2012, **48**, 15–21.
  - 39 C. Opreșan, V. Cârlescu, A. Barnea, G. Prisacaru, D. N. Olaru and G. Plesu, *Experimental determination of the Young's modulus for the fingers with application in prehension systems for small cylindrical objects*, IOP Conference Series: Materials Science and Engineering, 2016, vol. 147, no. 1, p. 012058.
  - 40 R. Moore, *J. Forensic Ident.*, 1989, **39**, 231–238.
  - 41 E. Degrandi-Contraires, C. Poulard, F. Restagno and L. Léger, *Faraday Discuss.*, 2012, **156**, 255–265.
  - 42 B. Murarash, Y. Itovich and M. Varenberg, *Soft Matter*, 2011, **7**, 5553–5557.
  - 43 H. John, F. Balszuweit, K. Kehe, F. Worek and H. Thiermann, *Handbook of Toxicology of Chemical Warfare Agents*, Academic Press, San Diego, 2009, pp. 755–790, DOI: 10.1016/B978-012374484-5.00050-X.
  - 44 A. Tiwari, L. Dorogin, A. Bennett, K. Schulze, W. Sawyer, M. Tahir, G. Heinrich and B. Persson, *Soft Matter*, 2017, **13**, 3602–3621.
  - 45 Y. Berdichevsky, J. Khandurina, A. Guttman and Y.-H. Lo, *Sens. Actuators, B*, 2004, **97**, 402–408.
  - 46 S. P. Jadhav, J. Wolfe and D. E. Feldman, *Nat. Neurosci.*, 2009, **12**, 792–800.
  - 47 X. Zhou, J. L. Mo, Y. Y. Li, J. Y. Xu, X. Zhang, S. Cai and Z. M. Jin, *Tribol. Int.*, 2018, **123**, 286–295.
  - 48 J. H. Cartwright, E. Hernández-García and O. Piro, *Phys. Rev. Lett.*, 1997, **79**, 527.
  - 49 J.-P. Vilotte, J. Schmittbuhl and S. Roux, *Non-Linearity and Breakdown in Soft Condensed Matter*, Springer, 1994, pp. 54–77.
  - 50 J. R. Rice, N. Lapusta and K. Ranjith, *J. Mech. Phys. Solids*, 2001, **49**, 1865–1898.
  - 51 S. S. Shroff, N. Ansari, W. Robert Ashurst and M. P. de Boer, *J. Appl. Phys.*, 2014, **116**, 244902.
  - 52 R. Williams and A. M. Goodman, *Appl. Phys. Lett.*, 1974, **25**, 531–532.
  - 53 A. Schallamach, *Wear*, 1971, **17**, 301–312.
  - 54 K. Viswanathan, N. K. Sundaram and S. Chandrasekar, *Soft Matter*, 2016, **12**, 5265–5275.